Science Reviews
from the end of the world

Vol. 1, No. 2, March 2020 // pp. 45-65 /

Modulation of Functional Features in Electron Transferring Metalloproteins

Daniel H. Murgida

Instituto de Química Física de los Materiales, Medio Ambiente y Energía (INQUIMAE), Departamento de Química Inorgánica, Analítica y Química Física, Facultad de Ciencias Exactas y Naturales, Universidad de Buenos Aires and CONICET, Buenos Aires, Argentina.
E-mail: dhmurgida@qi.fcen.uba.ar ORCID: 0000-0001-5173-0183

Abstract

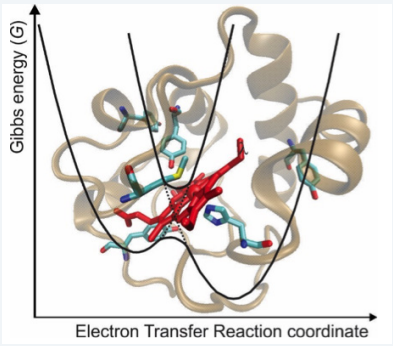

Electron transferring metalloproteins are typically implicated in shuttling electrons between energy transduction chains membrane complexes, such as in (aerobic and anaerobic) respiration and photosynthesis, among other functions. The thermodynamic and kinetic electron transfer parameters of the different metalloproteins need to be adjusted in each case to the specific demands, which can be quite diverse among organisms. Notably, biology utilizes very few metals, essentially iron and copper, to cover this broad range of redox needs imposed by biodiversity. Here, I will describe some crucial structural and dynamical characteristics that modulate the electron transfer parameters (and alternative functions) of two prototypical metalloproteins: the iron protein cytochrome *c* and its redox partner, the Cu_A center of the terminal respiratory enzyme cytochrome *c* oxidase. Specifically, I will focus on summarizing results obtained in recent years in my laboratory.

Keywords:
protein electron transfer, cytochrome *c*, copper A, metalloproteins, bioelectrochemistry, time-resolved SERRS spectroelectrochemistry.

Introduction

Electron transfer (ET) is the most elemental and one of the most ubiquitous chemical reactions in biology. Prototypical examples are the respiratory and photosynthetic ET chains that couple downhill ET reactions with uphill proton translocation across membranes to generate an electrochemical gradient that drives ATP synthesis. These processes often involve redox-active metal ions (and other cofactors) incorporated into a protein matrix (metalloproteins) as electron transporting or catalytic redox centers. The spectacular diversity of eukaryotic and prokaryotic life on Earth anticipates a wide palette of thermodynamic and kinetic redox needs to be covered by ET metalloproteins. Most surprisingly, nature employs very few metals, mainly iron and copper, to fulfill these divergent redox requirements,[1] thus indicating the existence of sophisticated ways of coarse and fine tuning of the relevant ET parameters, other than simply changing the redox active metal.

In this review, I will discuss these modulation mechanisms of thermodynamic and kinetic redox parameters for two specific cases: the (heme)iron protein cytochrome *c* (Cyt-c) and the copper protein Cu_A, which are redox partners in respiratory chains. The discussion is structured in terms of the modulation of individual parameters that, according to Marcus theory, determine ET efficiency.

The classical Marcus model relies on the transition-state theory and, therefore, assumes that reactants and solvent are in thermal equilibrium before the reaction.[2] The description is based on a two-state diagram where reactants and products are represented by intersecting free energy parabolas as a function of nuclear coordinates (Figure 1). Solvent thermal fluctuations eventually equalize reactants and products energy at the crossing point, thus enabling ET to render a product that is not yet equilibrated with the solvent. Note that this concept relies upon the underlying assumption that ET is much faster than solvent reorganization.

The parabolic shape of the two curves arises from the assumption that the medium can be described as an unsaturated dielectric continuum with linear polarization response. Both parabolas have identical curvature but are vertically and horizontally displaced with respect to each other, thus implying the following expression for the free energy of activation:

$$\Delta G^{\#} = \frac{(\Delta G^0+\lambda)^2}{4\lambda} \qquad \text{(Eq. 1)}$$

ΔG^0 is the thermodynamic driving force of the reaction (given by the difference of donor and acceptor reduction potentials, ΔE^0) and λ is the reorganization free energy, defined as the energy required for bringing the reactants from their equilibrium configuration to the equilibrium configuration of the products without actually transferring electrons (Figure 1).

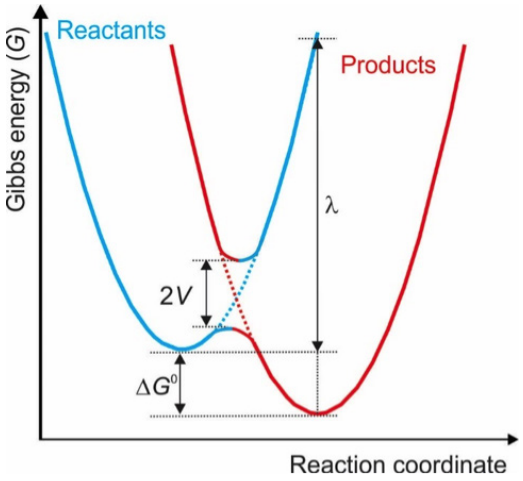

Figure 1. Energy diagram for electron transfer reactions according to Marcus model.

The introduction of quantum mechanical considerations to account for the possibility of classically forbidden electron tunneling leads to the most popular expression in protein ET, i.e. the high temperature limit of Marcus semiclassical expression for non-adiabatic ET reactions:

$$k_{NA} = \frac{2\pi V^2}{\hbar\sqrt{4\pi\lambda k_B T}} exp\left(\frac{-(\lambda+\Delta G^0)^2}{4\lambda k_B T}\right) \qquad \text{(Eq. 2)}$$

The pre-exponential term in Eq. 2 is the result of using Landau-Zerner theory for estimating the ET probability after one passage through the crossing point. Derivation of this expression recognizes that solvent (stochastic) fluctuations can be treated classically as they occur with low frequencies and, therefore, only high frequency vibrational modes of reactants and products need to be treated quantum-mechanically. Thus, assuming spherical ions in a polarizable continuum solvent, the reorganization energy can be separated into two contributions, $\lambda = \lambda_{vib} + \lambda_s$. Here λ_{vib} (also known as λ_{in}) corresponds to the reorganization of the redox active molecules, which can be estimated from the high frequency vibrational modes of reactants and products, whereas λ_s (also known as λ_{out}) accounts for the solvent reorganization and is estimated classically. Note that the dependence of k_{NA} with ΔG^0 leads to different regimes: the so-called normal, barrierless and inverted regions, which correspond to $0 \leq -\Delta G^0 \leq \lambda$, $-\Delta G^0 = \lambda$ and $-\Delta G^0 > \lambda$, respectively. Parameter V is the matrix element for the electronic coupling between reactant and product states, and its magnitude determines whether the ET reaction proceeds adiabatically or non-adiabatically. For sufficiently large V values (> 0.025 eV), the strong interaction

of the two parabolas results in two adiabatic surfaces separated by a magnitude $2V$ at the intersection point (Figure 1). In this case, the reaction evolves adiabatically along the lower surface trough the transition state and, therefore, its rate is independent of the value of V and limited by the probability of reaching the transition state. In the opposite limit of weak coupling (non-adiabatic ET), reaction rate is determined by the electron tunneling probability at the intersection point which, according to Eq. 2, scales with V^2.

In protein ET reactions, donor-acceptor distances are typically very long (> 10 Å), which results in very weak electronic couplings (see below) and, therefore, most experimental studies are rationalized in terms of Marcus semiclassical expression for non-adiabatic ET (Eq. 2). While this is certainly correct for most *in vitro* studies performed with diluted aqueous solutions (viscosity ≈ 1 *cP*), *in vivo* behavior can be drastically different since, for example, intracellular viscosities can be up to 500 times higher; therefore, long-range protein ET reactions are likely to be friction-controlled in spite of the weak coupling.[3,4]

As mentioned above, the electronic coupling matrix element V is a measure of the strength of interactions between reactants and products at the nuclear configuration of the transition state. For a precise description of V in proteins (and macrobiomolecules in general) it is necessary to account for its dependence on the distance between redox centers, on the dielectric properties and atomistic description of the insulating (or conducting) material in between, and on fluctuations of electronic and structural parameters at different levels and time-scales of the multidimensional and hierarchical free energy landscapes that characterize macromolecules. In a zero-order approach, one can approximate the medium that separates donor and acceptor as homogeneous and, therefore, the ET reaction can be treated in terms of a square barrier tunneling model. This assumption leads to an exponential decay of V as a function of the donor-acceptor distance r and of a medium-specific decay constant β:

$$V(r) = V(r_0)exp\left(-\frac{1}{2}\beta(r - r_0)\right) \qquad \text{(Eq. 3)}$$

To account for the structural complexity of proteins, Beratan and coworkers developed an extension of McConnell superexchange model, the so-called tunneling-pathway model.[5] In this approach, the medium between partner redox sites is broken into small subunits connected by covalent bonds, H-bonds and through space jumps, which differ in their ability to mediate coupling. Thus, the total coupling for a given pathway is estimated as a product of the couplings for the individual elements. The dependency expressed in Equation 3 remains valid, but the coupling decay parameter is now determined by the structural elements encountered along the pathway and, thus, the geometric donor-acceptor distance is replaced by an effective tunneling path length distance σ. Subsequent refinements retain some central points of the extended superexchange model, but incorporate more detailed and quantitative descriptions, particularly with regard to ultrafast dynamics.

The expressions discussed above refer to ET reactions between molecular redox partners. The description of electrochemical experiments of redox proteins is somewhat different, since one of the species involved is a solid electrode that can play the role of either donor or acceptor. In the case of redox species immobilized on the surface of metal electrodes, Marcus semiclassical expression needs to be integrated to account for all electronic levels in the metal:

$$k_{NA} = \frac{2\pi}{\hbar}V^2 \int_{-\infty}^{\infty} \frac{1}{1+\exp\left(\frac{\epsilon-\epsilon_f}{k_BT}\right)} \rho(\epsilon) \frac{1}{\sqrt{4\pi\lambda k_BT}} \exp\left[-\frac{(\lambda - e\eta + \epsilon)^2}{4\lambda k_BT}\right] \qquad \text{(Eq. 4)}$$

Note that in this case the reaction driving force can be set to the desired value (and sign) through the overpotential $\eta = E - E^0$, where E and E^0 represent the applied electrode potential and the redox potential of the molecular species, respectively. ρ is the density of electronic states in the electrode, the last term of the integrand is the Fermi-Dirac distribution law, ϵ_f is the energy of the Fermi level, and the remaining symbols have the usual meaning. This expression can be simplified by approximating the Fermi-Dirac distribution law as a step function:

$$k_{NA} \approx \frac{\pi}{\hbar}V^2 \,\mathrm{erfc}\left(\frac{\lambda + e\eta}{\sqrt{4\lambda k_BT}}\right) \qquad \text{(Eq. 5)}$$

In the following sections I will discuss, in relation to the specific cases of Cyt-c and Cu_A, the structural and dynamic features that modulate the relevant parameters that appear in equations 1 to 5, i.e. E^0, V and λ, and thereby the efficiency

of ET reactions in these proteins, as well as the regulation mechanisms that are beyond the scope of Marcus semiclassical theory.

1. Multifunctional cytochrome *c*

Mitochondrial cytochrome *c* (Cyt-c) is a globular and water-soluble monohemic protein that has an average size of 104 ± 10 amino acid residues, i.e. about 13 kDa, depending on the organism. The typical Cyt-c fold consists of five α-helices of different lengths interconnected by extended Ω loops, and a couple of short two-stranded antiparallel β-sheets (Figure 2). The slightly saddled heme group is covalently attached to two cysteine residues and buried into a hydrophobic pocket, with only one edge partially exposed to the solvent. The four N atoms of the porphyrin ring coordinate the iron ion equatorially, while residues His18 and Met80 serve as proximal and distal axial ligands, respectively.[6]

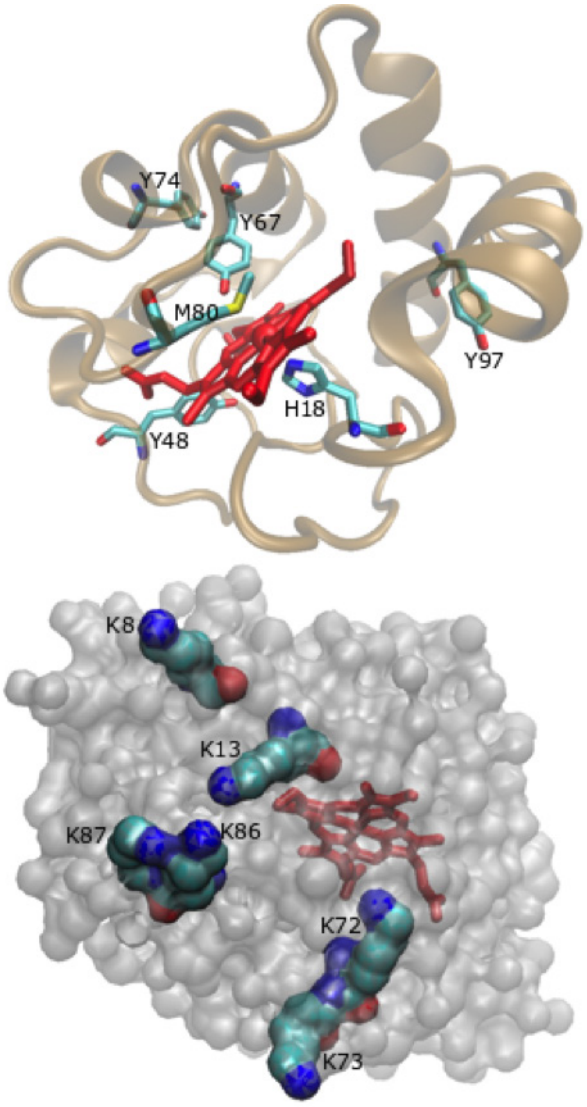

Figure 2. Crystal structure of horse heart ferric cytochrome *c* (PDBid 1HRC).[7] The top view shows the secondary structure elements, the two axial ligands and crucial tyrosine residues. The bottom view shows six surface lysine residues that constitute the binding site to natural redox partners and to negatively charged surfaces in general.

A comparison of crystallographic and NMR structures of the ferric and ferrous forms of Cyt-c indicate only subtle redox-linked conformational changes, which are mainly localized in the hydrogen-bonding network that involves one of the heme propionates, two crystallographic buried water molecules and side chains of several residues mainly on

the distal side. Spectroscopic studies, on the other hand, suggest higher flexibility of the ferric protein, which has been postulated as a key feature for regulating binding and dissociation to redox partners.

The structure described above corresponds to the so-called native conformation of Cyt-c, whose canonical function within the intermembrane space of mitochondria is shuttling electrons from complex III to the terminal respiratory enzyme cytochrome *c* oxidase (CcO), thus critically contributing to sustain cellular life. It should be noted, however, that Cyt-c behaves as a moonlighting protein, meaning that the actual function may change upon intracellular relocalization or post-translational modifications.[8] In response to aggressions such as DNA damage or metabolic stress, cells may activate complex and ordered sequences of cell suicide, known as apoptotic pathways. One of these sequences involves the release of mitochondrial Cyt-c into the cytosol. After the relocalization, Cyt-c forms a complex with the cytosolic protein Apaf-1, which triggers a cascade of caspase activation events that ends up in cellular death. Moreover, once in the cytosol Cyt-c may translocate into the nucleus in response to DNA damage and block cell survival by impeding nucleosome assembly. Interestingly, Cyt-c can be the architect of its own liberation to the cytosol through the permeabilization of the mitochondrial membrane. In this case, the interaction of the protein with the membrane component cardiolipin (CL) induces a conformational transition that results in the gain of peroxidatic activity towards CL.[9] Post-translational modifications of Cyt-c observed under oxidative stress conditions may either favor the gain of peroxidatic activity or interfere with the binding to CL and Apaf-1, suggesting a complex interplay of pro- and antiapoptotic stimuli.[6,8–11] Translocation mechanisms and the conformational details associated to each alternative function of Cyt-c remain largely unknown, but there is certain consensus that the conserved structural flexibility of this protein is central to its tunable functionality.

1.1. Redox thermodynamics of Cyt-c

Redox potentials (E^0) of type *c* cytochromes in general (including eukaryotes, bacteria and archaea) cover a very broad range from ca. -500 mV to 500 mV, thus highlighting the tunability of the common metalloporphyrin redox active site.[6] A careful inspection of the structural differences between cytochromes allows dissecting the main structural determinants and their relative contributions to E^0, as schematically summarized in Figure 3.

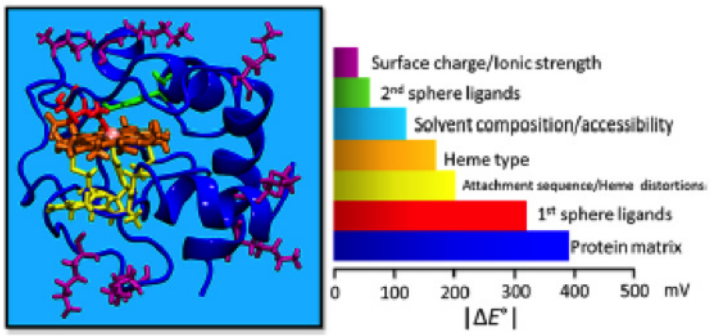

Figure 3. Structural elements that contribute to different extents to tune the redox potential of Cyt-c. Adopted from reference 6 with permission. Copyright 2017, American Chemical Society.

The first coordination sphere of the metal ion is probably the most crucial determinant of E^0. Thus, the tetradentate equatorial ligand has a strong influence on the differential stabilization of Fe^{2+} versus Fe^{3+}, which in turn is syntonized by the electron donation/withdrawing properties of the porphyrin substituents. An even stronger effect is exerted by the axial ligands, Met80 and His18 in native Cyt-c. The π-electron-acceptor character of the thioether sulfur atom in Met80, as well as the burial of the heme within a hydrophobic pocket and its concomitant poor solvent accessibility, stabilizes Fe^{2+} relative to Fe^{3+}. Therefore, the detachment of Met80 and the increased solvent accessibility that characterizes most alternative conformations of Cyt-c results in large downshifts of E^0 of up to 400 mV, which can be partially ascribed to the loss of Fe^{2+} stabilization.[8,12–14] Under these conditions, Cyt-c is unable to efficiently shuttle electrons in the respiratory chain, but instead acquires redox and structural characteristics typical of a peroxidase.

The heme moiety is embedded in a largely fluctuating amino acidic matrix that may dynamically modulate the electronic properties of the site through specific first and second sphere interactions, through the local electrostatic potential, and by imposition of deformation of the tetrapyrrol from planarity. Thus, the thermodynamic and kinetic redox parameters

of Cyt-c are sensitive to changes in a number of structural elements, which in turn can be affected by interactions with redox partners in reactive complexes, by the nature and ionic composition of the solvent as well as by pH and temperature.

1.2. Kinetic electron transfer parameters of Cyt-c

Given that most protein ET reactions occur under very small thermodynamic driving forces ($\Delta G^0 \sim 0$), metal redox centers have structurally evolved in order to minimize λ, thereby maximizing the ET rate. In the case of Cyt-c, experimental evidence points out that the same structural features that optimize E^0 (see section 1.1) are also responsible for minimizing λ, as essentially every structural perturbation of the WT protein results in a rise of this parameter. For example, replacement of the axial ligand Met80 by an exogenous pyridinil ligand, or its mutation for a non-coordinating alanine residue, leads to a ca. two-fold increase of λ.[15] A similar effect is observed upon addition of urea due to augmented solvent exposure of the metal site in the partially unfolded protein.

Interestingly, electrostatic interactions of Cyt-c with model systems have also been found to modulate the magnitude of λ.[16,17] Computational and experimental studies demonstrated that Cyt-c utilizes a patch of positively charged Lys residues that surround the partially exposed heme edge for electrostatic binding to partner proteins, such as Cyt-c oxidase, reductase and peroxidase. The same set of Lys residues was found to constitute de binding site to metal electrodes coated with self-assembled monolayers (SAMs) of carboxyl-terminated alkanethiols, thus validating the use of these simplified model systems for assessing the effect of electrostatic interactions on ET parameters.[18,19] The use of these simple SAM/Cyt-c models presents a number of important advantages: (a) the protein adsorbs with the heme edge facing the SAM, which allows for efficient direct electrochemistry; (b) surface confinement prevents diffusional control, thus facilitating the determination of relevant kinetic parameters; (c) the electrode functions as either electron donor or acceptor and the ET driving force can be tuned trough the electrode potential; (d) the electronic coupling can be easily varied though the chain length of the alkanetiols; (e) the interfacial electric field can be systematically varied trough parameters such as electrode potential, chemical composition of the SAM (i.e. density of charged head groups and chain lengths), pH and ionic strength. It has been demonstrated, both theoretically and experimentally, that the interfacial electric fields in these model systems are of the same magnitude as in biological membranes.[12,20–22] Furthermore, if the surfaces of the Au or Ag electrodes are nanostructured previous to the SAM-coating process, these modified surfaces behave as suitable platforms for surface-enhanced (resonance) Raman (SER/SERR) detection of the adsorbed Cyt-c.[13,23] Thus, thermodynamic and kinetic ET parameters can be obtained from spectral deconvolution of stationary or time-resolved potential-dependent SERR measurements, respectively. This methodology has the advantage over conventional electrochemical techniques of providing real time structural information of the immobilized protein under reactive conditions. Moreover, the method allows obtaining a precise determination of λ from the overpotential dependence of the ET rate constant measured by TR-SERR at constant temperature (see Eq. 5). This type of experiments revealed that the reorganization energy of Cyt-c electrostatically adsorbed on COOH-terminated SAMs under conditions that preserve the native structure is only a half of the value determined for the WT protein in solution, i.e. 0.3 and 0.6 eV, respectively. In contrast, the Tyr67Phe mutant, which lacks the native Tyr67-Met80 hydrogen bonding interaction, yields λ = 0.3 eV irrespectively of the interfacial electrostatic field.[17] These results, in combination with molecular dynamic simulations, revealed that the local electrostatic field induces subtle deformations of the flexible Ω loops that contain most of the Lys residues that constitute the protein binding site. Such minor distortions neither represent a measurable change of secondary structure nor affect the first coordination sphere of the heme iron. However, they affect the H-bonding network to some extent, thus altering the interactions between first and second coordination sphere residues. Most notably, electrostatic interactions disrupt the Tyr67-Met80 H-bond in a similar fashion as the Tyr67Phe mutation, which results in the minimization of λ without affecting E^0.[17] Based on these findings, it was proposed that a similar electrostatically driven switch between Cyt-c native forms of high and low λ might also be triggered upon a binding of Cyt-c to the natural redox partners. I will come back to this important point in section 3.

Interestingly, the finding that Cyt-c may exist in two alternative native forms that differ in λ and whose interconversion is driven by the electrostatic field allows rationalizing the large dispersion of λ values reported in the literature for type *c* cytochromes. Indeed, the average λ taken over all values reported for Cyt-c samples from different organisms in solution (i.e. with no field applied) is ca. 0.6 eV. This average number drops to ca. 0.3 eV when taken over electrostatic complexes of Cyt-c. Moreover, the different Cyt-c variants reported so far can be classified into high and low λ forms depending on the presence or absence of the Tyr67−Met80 H-bond, respectively.

Residue Tyr67 is not only crucial for regulating λ, mutation of this residue has also been found to significantly affect the electronic coupling (V) between the heme group and an artificial redox probe. This is true even for the conservative Tyr67Phe mutant, for which simple pathways calculations do not predict significant differences, but quantum mechanical calculations predict that altered dynamics of the aromatic ring translate into lower V due to less favorable orbital overlap

between the aromatic ring of Tyr67 and the heme.[24] Another factor that has been proposed to affect *V* is the heme ruffling, since increasing out-of-plane distortion decreases delocalization of the Fe $3d_{\pi}$-based molecular orbitals onto the β-pyrrole carbons.[25] In addition to these fine-tuning mechanisms, the most important determinants of the electronic coupling between Cyt-c and its redox partners are the structure and dynamics of the inter-protein complexes, as highlighted by electrochemical and spectroelectrochemical experiments of Cyt-c immobilized on SAM-coated electrodes.[18,19,26–30] The electrochemical determination of apparent ET rate constants (k_{ET}^{app}) for Cyt-c and other redox proteins adsorbed on variable thickness SAMs revealed distance dependencies that cannot be explained in terms of Marcus theory.[31] This behavior is characterized by the expected exponential decay of k_{ET}^{app} with the Cyt-c/electrode distance (number of -CH_2- groups in the SAMs) only for alkanethiols with more than 10 -CH_2- groups, with a coupling decay constant consistent with a reaction rate limited by through-bond electron tunneling probability ($\beta \approx 1$ per -CH_2- group). For thinner SAMs, in contrast, k_{ET}^{app} has much softer distance dependence and tends to plateau. This change of ET regime for electrostatically adsorbed Cyt-c was investigated by time-resolved surfaced-enhanced resonance Raman (TR-SERR) spectroelectrochemistry taking advantage of the surface selection rules, which allow for monitoring the coarse reorientation of Cyt-c simultaneously with its redox state and heme pocket structure.[26] The experiments revealed a dynamic behavior (rotational diffusion) of the adsorbed Cyt-c molecules. In thicker SAMs, this motion is four orders of magnitude faster than the redox reaction, thus confirming a non-adiabatic ET mechanism at these tunneling distances. In thinner SAMs, protein reorientation rate is slowed down drastically and becomes similar to k_{ET}^{app}, indicating that the overall redox reaction rate is limited by protein reorientation. Interestingly, molecular dynamics simulations combined with pathways calculations reveal that the most stable orientation of Cyt-c in the electrostatic complex does not provide an efficient pathway for heterogeneous ET (Figure 4), thereby suggesting that protein reorientation is a prerequisite for the reaction.[18,19]

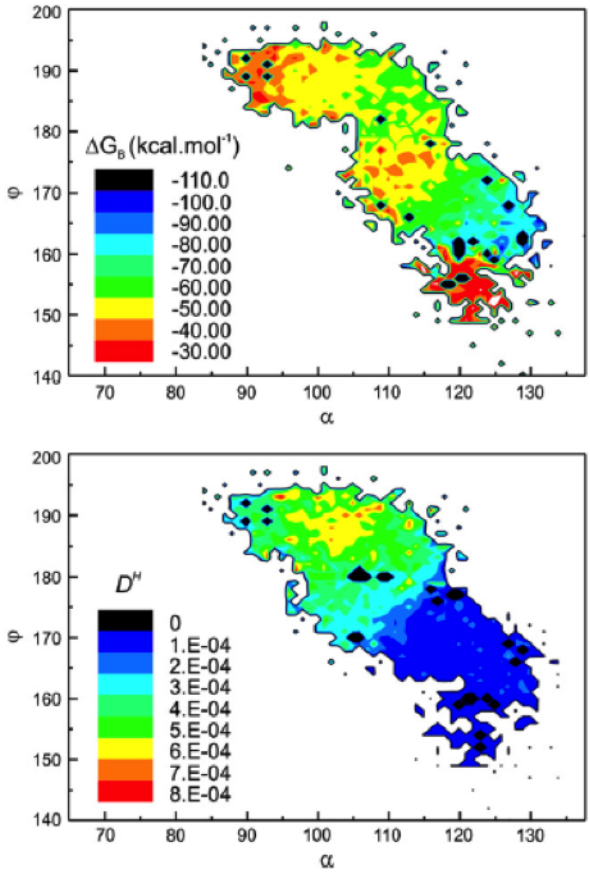

Figure 4. Binding energy (top) and electronic coupling of Cyt-c adsorbed on electrodes coated with COOH-terminated SAMs as a function of angles α and ϕ, which define the orientation of the heme with respect to the electrode surface. Note that optimal binding is achieved for (α, ϕ) values around (128, 165), while optimal coupling requires reorientation to values around (105, 188). Adopted from reference [32] with permission. Copyright 2014, Elsevier B.V.

Thinner SAMs imply higher tunneling probabilities but also higher local electric fields that slow down protein reorientation. Thus, upon shortening the chain length of the SAMs, the redox process becomes kinetically gated by reorientational dynamics. In agreement with this interpretation, mutation of the key amino acid Lys87 (Lys87Cys mutant), which stabilizes low-coupling orientations, results in the recovery of an exponential distance dependence of k_{ET}^{app} for all chain lengths.[30] In addition to coarse protein orientation, subtle fluctuations such as the movement of interfacial water molecules and side-chain rearrangements may also have a deep impact on coupling. Indeed, cross-linking of Cyt-c to the SAMs results in fixed coarse orientation and hindered protein reorientation, but the anomalous distance dependence is still verified, suggesting that both coarse and fine dynamics are strongly affected by interfacial electric fields of biologically relevant magnitude.[28] The potential biological impact of these findings will be discussed in section 3.

A different explanation for the unusual distance-dependence of k_{ET}^{app} consists of a changeover of ET regime from non-adiabatic at long distances to friction control at the thinner SAMs. The experimental signature of the friction control regime is a viscosity-dependent k_{ET}^{app}, which, however, is also expected in the case of a gating step such as protein reorientation. An elegant strategy to suppress reorientation is direct wiring of the heme iron to the electrode by using SAMs that include pyiridinil-terminated alkanethiols, which have been shown to displace the native Met80 ligand.[33] For these systems, a gating step in the plateau region (thinner SAMs) can be safely discarded as the value of k_{ET}^{app} measured at constant temperature by TR-SERR displays a clear dependence with the applied overpotential, yielding λ values above 0.5 eV.[15] This behavior contrasts with the flat overpotential dependence of k_{ET}^{app} for Cyt-c electrostatically adsorbed on thin SAMs with high negative charge density.[13] Thus, the most likely scenario is that both electric-field-modulated large and small amplitude motions (i.e., a reorientation, water rearrangement, etc.) and the onset of friction control may both play a role in regulating the kinetic behavior of Cyt-c depending on the specific conditions.

1.3. Redox coupled conformational changes of Cyt-*c*

In the preceding sections, I have centered the discussion around the canonical electron shuttling function of Cyt-c that is associated with the so-called native protein structure, i.e. the one derived from crystallography at neutral pH. It should be noted, however, that this static picture corresponds to a minimum of a multidimensional free energy landscape that includes other sub-states that are energetically accessible at physiological temperatures. Moreover, a number of environmental conditions may alter either the free energy landscape or the conformational diffusion parameters that determine landscape exploration.[6,8] In the mitochondrial intermembrane space, such conditions include crowding effects, local electric fields and altered local pH values, as well as specific and unspecific protein-protein and protein-lipid interactions. These effects may be crucial in fine-tuning ET parameters, but may also result in alternative Cyt-c conformations with different functionalities. Indeed, it has been extensively demonstrated that these types of perturbations affect Cyt-c structure in different ways, but always including the disruption of the Met80-Fe bond as one of the primary events.[6,8,9,14,34] Additionally, the disruption of this bond under mild perturbation has been found to take place preferentially in ferric Cyt-c, and only rarely in the ferrous protein. This difference has long been ascribed to the lower strength of Fe^{3+}-S(Met) compared to Fe^{2+}-S(Met). Recent resonance inelastic X-ray scattering studies, however, demonstrated the opposite trend in redox state-dependent bond strengths, and indicated that 50% of the bond stabilization in the ferric protein arises from contributions of the protein scaffold, probably involving the network of H-bond interactions.[35,36] Consistent with this, quantum mechanical calculations show that the experimentally observed disruption of the same bond by biologically meaningful external electric fields cannot be ascribed to a field-induced weakening of the bond.[37] Instead, simulations show that exposure to moderate electric fields results in distortion and increased flexibility of crucial protein segments due to polarization and alignment with the field.[38] Moreover, calculations show that the application of electric fields favors the pentacoordinated form both energetically and entropically, and also lowers the activation barrier of the process.

The most thoroughly studied alternative conformation of Cyt-c is the so-called alkaline form, whose main characteristic is the replacement of the axial Met80 ligand by a surface Lys residue to produce a six-coordinated low spin (6cLS) conformation with Lys/His axial coordination pattern.[6,8] For the most studied equine Cyt-c, this transition has a $pK_a = 9.4$ and the distal axial ligand at $pH > pK_a$ can be either Lys79 or Lys73. Structural models show that the largest structural differences of the alkaline conformation with respect to native Cyt-c are localized in the regions that exhibit increased conformational dynamics in the ferric protein with respect to the ferrous one, which may explain why the alkaline transition is only observed for oxidized Cyt-c.[39,40] In the alkaline conformation, the redox potential is downshifted by 300 mV, rendering the protein unable to function as electron shuttle.[14] This change is accompanied by a gain of peroxidase activity, most likely ascribable to a dynamic equilibrium with minor amounts of five-coordinated high-spin species.[10] In this respect, the alkaline transition represents a paradigmatic case of function gaining. The minimal mechanism for the transition includes deprotonation of an unknown triggering residue, followed by ligand exchange.

Recent TR-SERR studies identify Lys73 as the most likely triggering group and show that electrostatic interactions of Cyt-c with biomimetic surfaces shift the pK_a of the transition to even higher values.[14] Thus, the unphysiologically high pK_a of this process makes the alkaline conformation interesting for basic biophysical studies, but unlikely to be biologically relevant. Recent findings, however, show that certain post-translational modifications and naturally occurring mutations of mammalian Cyt-c have the effect of downshifting the pK_a of the alkaline transition towards physiological pH, making this process potentially relevant *in vivo*.[6,8] One of these modifications is naturally occurring Tyr74 nitration, which results in deprotonation of the phenolic ring at neutral pH, concomitant with Met → Lys axial ligand exchange with pK_a values of 7.1 and 8.9 for the protein free in solution and electrostatically adsorbed on SAM-coated electrodes, respectively.[10,41] Computational studies suggest that the change of electrostatic field caused by deprotonation of nitro-Tyr74 as triggering event stabilizes the Lys/His form relative to the intermediate pentacoordinated species, thereby increasing the activation barrier for the inverse Lys → Met ligand exchange,[10] as also experimentally verified by TR-SERR.[14]

The alkaline conformation is only one of many alternative conformations reported for Cyt-c. A large number of studies have demonstrated that, even at neutral pH, electrostatic interactions of Cyt-c with a variety of negatively charged model systems – including phospholipid vesicles, micelles, polyanions, and others – induce conformational changes that involve the disruption of the labile Met80-Fe bond, mainly in the ferric form.[6,34] As a result of these interactions, the distal axial position may remain vacant, leading to a penta-coordinated high-spin species (5cHS; with His18 proximal coordination), or be occupied by either His26 or His33, leading to a hexa-coordinated low-spin form (6cLS; with His23,33/His18). Eventually, and depending on the specific conditions, small amounts of a hexa-coordinate high-spin form with H_2O/His18 axial coordination can also be found.[34] These alternative conformations have very low redox potentials compared to the native form, and are often referred to as B2 conformations.[42] Systematic studies have shown that the amount of B2 forms in equilibrium with the native conformation correlate with the strength of the interfacial electrostatic field in the complexes.[12]

The interaction of Cyt-c with cardiolipin (CL) containing liposomes is particularly relevant, since CL is the only anionic phospholipid present in the inner and outer mitochondrial membranes. Actually, about 15 % of the mitochondrial Cyt-c is bound to CL in healthy cells. The binding of Cyt-c to CL has been extensively studied, but with contradicting results regarding the heme structure in the complexes.[9,43] Recent resonance Raman studies demonstrated that the interaction of native Cyt-c with CL induces a ligand exchange to produce a B2 species with His/His axial coordination pattern, where the proximal position is occupied by the native His18 ligand, and the distal one corresponds to either His33 or His26 (Figure 5).[9] Interestingly, this CL-induced transition is not restricted to native Cyt-c. Alternative conformations of Cyt-c, such as those with Lys/His and OH^-/His axial coordination patterns stabilized by post-translational Tyr74 nitration and Met80 sulfoxidation, respectively,[10,11] also lead to spectroscopically identical His/His species (Figure 5).[9]

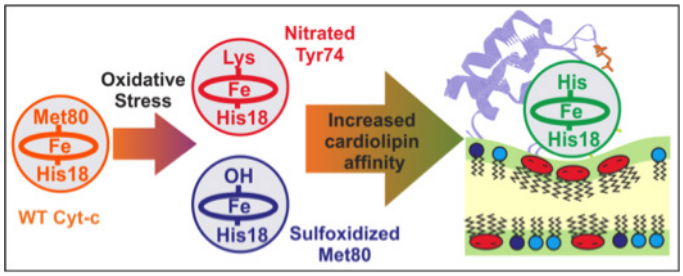

Figure 5. Schematic representation of cardiolipin-induced conformational changes of wild type Cyt-c and post-translationally modified forms of the protein. Adopted from reference[9] with permission. Copyright 2015, American Chemical Society.

The His/His alternative conformation presents an apparent peroxidase activity 15 times higher than the Met/His native form, and twice larger than the Lys/His and OH^-/His conformations. This activity is ascribed to the lability of the distal His ligand in the His/His complex, which is in equilibrium with small but detectable amounts of enzymatically competent high spin species. Moreover, the nitration of Tyr74 and sulfoxidation of Met80 result in a 4-fold enhancement of the binding affinity of Cyt-c to CL, suggesting that these translational modifications amplify the pro-apoptotic signal.[9] Moreover, it was recently shown that inorganic and organic phosphate anions efficiently mediate the binding of Cyt-c to the abundant zwitterionic lipids in membrane phosphatidylcholine and phosphatidylethanolamine. In these complexes, Cyt-c reacts efficiently with H_2O_2 at submillimolar levels, which oxidizes the sulfur atom of the axial ligand Met80.[11] Thus, the rise of H_2O_2 to submillimolar concentrations that characterizes the early stages of apoptosis produces a post-translational

modification of Cyt-c with enhanced affinity for CL and enhanced CL-peroxidase activity, thus facilitating membrane permeabilization as a crucial part of the apoptotic program.

2. Cytochrome *c* oxidase

Cytochrome *c* oxidase (CcO), also known as respiratory complex IV, is an integral membrane protein that serves as terminal electron acceptor in aerobic respiratory chains in mitochondria and bacteria. The enzyme accepts four electrons from Cyt-c and employs their excess free energy to translocate four protons across the membrane, thus contributing to generate the electrochemical gradient that drives ATP synthesis. Finally, electrons are transferred to the sacrificial acceptor O_2, producing H_2O as a by-product. The size and detailed structure of CcO is organism-dependent, but all canonical enzymes contain two copper and two heme centers. A Cu_A site accepts electrons from Cyt-c redirecting them to a heme *a* or *b* cofactor, and from there to the heme a_3 / Cu_B binuclear site, where O_2-reduction is catalyzed. Mammalian CcO enzymes are large and complex structures composed of 13 subunits. In contrast, bacterial enzymes are largely simplified versions that typically contain only 4 subunits, with the three largest subunits (I, II and III) highly homologous to the mitochondrion-encoded components that form the catalytic core of the enzyme. For example, the ba_3-CcO from *Thermus thermophilus* is a 85 kDa membrane integral protein complex that features three subunits forming a bundle of 15 transmembrane helices. From these helices, 13 belong to the large subunit I, which contains hemes *b* and a_3, as well as Cu_B, while subunit II is composed of a transmembrane helix and the Cu_A-containing periplasmic domain (Figure 6). The high homology verified at the levels of subunits I and II renders bacterial complexes as suitable model systems of the more complex eukaryotic enzymes.

In the following sections, I will focus on the primary electron acceptor in CcO, i.e. the Cu_A-containing protein fragment in subunit II, with some emphasis in recent results obtained with the fragment from *Thermus thermophilus* ba_3-CcO (*Tt*-Cu_A hereafter).

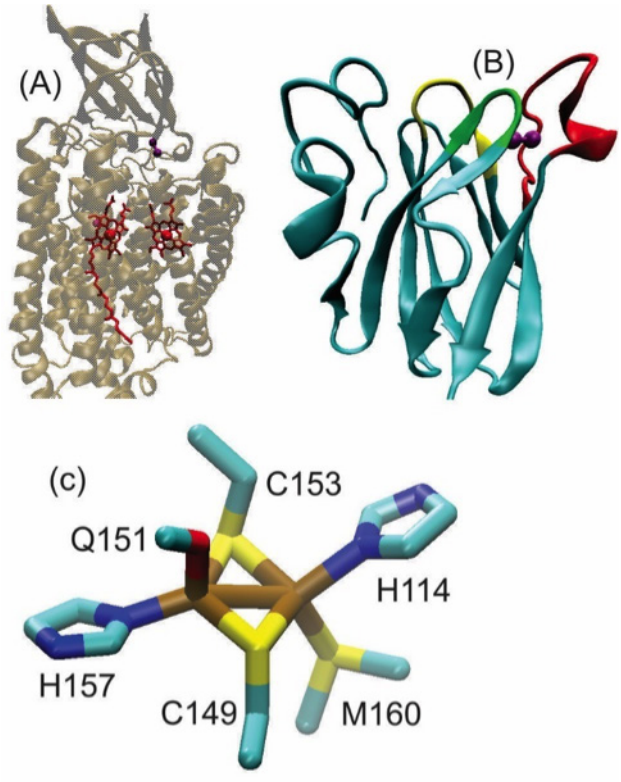

Figure 6. Crystal structures of the ba_3 CcO from *Thermus thermophilus*. (a) Structure of the integral enzyme (PDBid 3EH5).[44] (B) Cu_A-containing soluble fragment in subunit II (PDBid 2CUA). (C) Detailed view of the Cu_A site (PDBid 2CUA).[45]

2.1. Structure and electronic properties of Cu_A

The Cu_A site constitutes the primary electron acceptor of most eukaryotic and prokaryotic CcO enzymes, as well as of N_2O-reductases involved in the nitrogen cycle. It functions as a highly efficient redox hub that redirects the electrons provided by a soluble redox shuttle by nearly 90°, thus linking inter- and intramolecular ET reactions.

The structure of Cu_A is highly conserved and features two copper ions bridged by two Cys ligands forming a nearly planar Cu_2S_2 diamond core structure. Both coppers are further coordinated by one equatorial His strong ligand and by one weak axial ligand, a Met sulfur and a backbone carbonyl, respectively (Figure 6). The metal ions are surrounded by three loops of conserved length that contain the also conserved ligand set and differ among species in the noncoordinating residues only.[45]

Despite containing two copper ions, Cu_A behaves as a one-electron redox couple alternating between a paramagnetic and fully delocalized mixed-valence pair $Cu^{1.5+}$–$Cu^{1.5+}$ and a diamagnetic reduced state, Cu^{+}–Cu^{+}. This property can be ascribed to the unique metal–metal bond found in Cu_A, which has a length of ca. 2.4-2.5 Å. The resulting delocalized unpaired electron in the oxidized center is coupled with two equivalent copper ions with nuclear spin I = 3/2, which produces a characteristic seven-line hyperfine splitting pattern in the EPR spectra.[46]

Oxidized Cu_A is purple as a result of two intense absorbance bands at ca. 480 and 530 nm assigned to S(Cys)→Cu charge transfers, and a broad band at ca. 760–800 nm assigned to intervalence charge transfer. Reduced Cu_A, in contrast, is colorless due to the d^{10} electronic configuration of both copper ions.

The electronic structure of the $Cu^{1.5+}$–$Cu^{1.5+}$ site has been described in terms of an adiabatic double-well potential energy surface as a function of small geometric perturbations such as the Cu-Cu distance. The lower energy well is associated to a molecular orbital description featuring a σ_u* highest occupied molecular orbital (HOMO), and corresponds to the crystallographic Cu-Cu distance of about 2.4 Å. The second well is slightly more energetic but still thermally accessible, and it is associated to an elongated metal-metal bond and to a π_u HOMO symmetry.[47] Because of their thermal interconversion, the two wells are often designated as σ_u* and π_u alternative electronic ground states (GS), and the energy difference between them is the energy gap $\Delta E_{\sigma_u^*/\pi_u}$. Quantum mechanical calculations show that, in addition to Cu-Cu stretching, other perturbations, such as dihedral distortions or the application of biologically meaningful electric fields, may also affect $\Delta E_{\sigma_u^*/\pi_u}$ and, therefore, the relative populations of both GS.[48]

Because of the overlapping spectroscopic features of the multiple metal centers in N_2O-reductases and CcO enzymes, the detailed physicochemical characterization of Cu_A centers requires simplified model systems. Two important strategies along these lines are (i) producing truncates of native CcO proteins containing intact Cu_A sites and (ii) engineering artificial Cu_A sites into small soluble proteins. The most extensively studied examples in each case are the Cu_A-containing soluble fragment of the ba_3-CcO from *Thermus thermophilus* (*Tt*-Cu_A) and the Cu_A site engineered into azurin from *Pseudomonas aeruginosa* (*Pa*-Azu-Cu_A).[1] The first model, *Tt*-Cu_A, is particularly appealing because it is highly stable and, according to the available structural and spectroscopic characterization, it retains all the characteristic features of the Cu_A site in the integral enzyme and, therefore, can be regarded as a native Cu_A center. In recent years, the *Tt*-Cu_A site has been engineered to produce a variety of mutants at different structural levels to introduce perturbations that help elucidating the structural basis of the functional features. The different *Tt*-Cu_A variants produced are summarized in Table 1.

Table 1. Cu_A chimeras constructed by either single or multiple mutations of *Tt*-Cu_A at the level of the three loops that surround the metal site (see Figure 6)

Modification	Name	Loop 1 (86-89)	Loop 2 (110-115)	Loop 3 (149-160)	E^0 (mV)
None (wild type)	*Tt*-Cu_A	FAFG	PDVIHG	CNQYCGLGHQNM	261
1st sphere mutants	M160H	FAFG	PDVIHG	CNQYCGLGHQNH	79
	M160S	FAFG	PDVIHG	CNQYCGLGHQNS	177
	M160Y	FAFG	PDVIHG	CNQYCGLGHQNY	316
	M160L	FAFG	PDVIHG	CNQYCGLGHQNL	314
	M160Q	FAFG	PDVIHG	CNQYCGLGHQNQ	93
2nd sphere mutant	*Tt*-1L-E	HQWY	PDVIHG	CNQYCGLGHQNM	297
	Tt-1L-L	FAFG	PDVIHG	CSEICGANHSNM	226
	Tt-3L-*Hs*	HQWY	QDVLHG	CSEICGANHSNM	242
	Tt-3L-*At*	HQWY	SADVLHG	CSEICGTNHAFM	241
1st + 2nd sphere mutations	*Tt*-3L-M160H	HQWY	QDVLHG	CSEICGANHSNH	74

As modification of the strong Cys and His ligands of the Cu_A site are known to be disruptive, first coordination sphere modifications were restricted to the replacement of the weak axial ligand Met160 by a variety of amino acids.[3,48–54] Second sphere modifications, on the other hand, were accomplished by replacement of either one or the three loops that surround the metal site (Figures 6 and Table 1) by the homologous sequences from *Homo sapiens* and *Arabidopsis thaliana* with preservation of the conserved ligand set.[50,54] Moreover, combined first and second coordination sphere modification was achieved by introducing the Met160His point mutation in the so-called *Tt*-3L-*Hs* chimera.[53] In all cases, the generated proteins were characterized by a variety of spectroscopic methods such as UV-vis, EPR, NMR, RR and EXAFS, which demonstrate that the structure and the mixed valence character of the Cu_A site are preserved in all these variants. Interestingly, a comparison of the UV-vis spectra obtained experimentally and calculated by TD-DFT indicate that the different modifications alter the relative populations of the alternative σ_u^* and π_u ground states, i.e. modulate the size of $\Delta E_{\sigma_u^*/\pi_u}$ and, therefore, the thermal accessibility of the more energetic π_u ground state. In agreement with this interpretation, UV-vis spectra recorded as a function of temperature display changes of relative intensities that are consistent with varying Boltzmann populations. Some of the ^1H and ^{13}C NMR chemical shifts of the oxidized Cu_A centers exhibit an anti-Curie temperature dependence that reflects the Boltzmann-like relative populations of the alternative σ_u^* and π_u ground states. Quantitative treatment of these temperature dependencies in terms of a two-states model yields a measure of $\Delta E_{\sigma_u^*/\pi_u}$. As summarized in Figure 7, first and second sphere perturbations result in strong modulation of $\Delta E_{\sigma_u^*/\pi_u}$ and, moreover, the two effects display some degree of additivity. The $\Delta E_{\sigma_u^*/\pi_u}$ measured for the WT *Tt*-Cu_A site is 600 cm^{-1}, which implies 95:5 relative populations of the σ_u^* and π_u states at room temperature. This gap could be increased up to ca. 900 cm^{-1} to obtain π_u populations of 1% only, and decreased to virtually zero to obtain degenerate σ_u^* and π_u ground states.

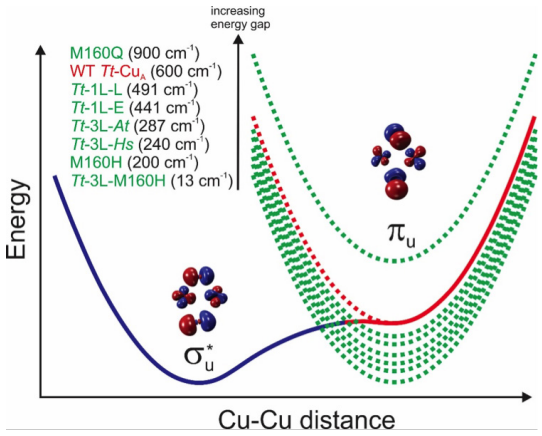

Figure 7. Schematic representation of the two-well potential energy surface of the Cu_A site as a function of the Cu-Cu coordinate. The different modifications summarized in Table 1 tune the energy gap ($\Delta E_{\sigma_u^*/\pi_u}$) between the two wells.

2.2. Redox thermodynamics of Cu_A

Reduction potentials have been experimentally determined for a variety of model Cu_A centers that include: (i) detergent solubilized integral CcO and N_2O-reductase wild type enzymes, (ii) Cu_A-containing soluble fragments of CcO subunit II and (iii) artificial Cu_A sites engineered into the scaffold of small soluble cupredoxins. The average E^0 taken over all values reported so far is 256 ± 80 mV. Given that the ligand set is preserved in all cases, the ±80 mV variability probably reflects differences in the protein milieu, although experimental variability may also play a role.

Interestingly, in the case of the chimeric protein *Pa*-Azu-Cu_A, $E°$ was found to upshift by 180 mV upon lowering pH from 7 to 4. EPR spectra exhibit concomitant drastic changes that suggest either a transition from mixed valence to localized valence or a slight change of wavefunction composition of the mixed valence complex induced by protonation at pH 4.[55,56] These results lead to a novel feedback inhibition mechanism for the activity of CcO. The ET-driven proton pumping activity of CcO is postulated to result in protonation and detachment of this His ligand, thus inducing a drastic upshift of E^0 that impairs ET and, thus, arrests CcO activity until protons are released into the outer membrane space and the His residue is deprotonated. This ground-breaking proposal, however, collides with a later finding that underlines the, until then overlooked, importance of the protein matrix: in the native *Tt*-Cu_A, a similar change of pH results in a modest 15 mV variation of E^0.[57] Moreover, eight different variants of *Tt*-Cu_A, generated either by single point mutation or by loop engineering, display upshifts of only 8-58 mV upon lowering pH from 7 to 3.5.[54] Most likely, the sharp contrast between the two model systems arises from the presence of a protonable residue, His35, in the artificial *Pa*-Azu-Cu_A construct that is not present in the native *Tt*-Cu_A protein.

In addition to the overall protein fold effect, first coordination sphere ligands exert a strong influence on E^0. For example, the thiolate ligands that constitute the Cu_2S_2 diamond strongly stabilize the oxidized form of Cu_A. When compared to T1 mononuclear copper centers this strong stabilization is expected to result in E^0 values lower than the average 256 mV, suggesting that valence delocalization partially compensates this effect relative to a trapped mixed-valence dimer. Also, the strong His equatorial ligands drastically affect E^0 and the electronic description of the center in general, as shown for the His260Asn mutant of the integral CcO from *Rhodobacter sphaeroides*. Mutation of the weak axial ligands, in contrast, is expected to be less disruptive in terms of the electronic structure, which also anticipates weaker modulation of E^0. This has been experimentally verified for the *Pa*-Azu-Cu_A model. On one hand, the esterification of the backbone carbonyl in Glu114 (weak axial ligand) has no effect on E^0.[58] Mutation of the other weak axial ligand Met, on the other hand, results in minor variations of E^0 of about 5 to 16 mV only.[59] However, in sharp contrast with this, equivalent mutations introduced in integral CcOs from *Rhodobacter sphaeroides* and from *Paracoccus denitrificans* shift E^0 by ca. 100-120 mV,[60,61] once again highlighting the importance of the overall protein scaffold in scaling the influence of first sphere ligands. The systematic mutation of the equivalent Met ligand in the soluble *Tt*-Cu_A fragment confirms this view, as it results in strong modulation of E^0 (Table 1) without affecting mixed valence delocalization.[49] Temperature-dependent electrochemical determinations for the different *Tt*-Cu_A variants reveal partial compensation of the enthalpic and entropic contributions that attenuate E^0 variations to some extent. Yet, E^0 values show a good linear correlation with the hydrophobicity of the weak axial ligand that can be associated to coulombic stabilization/destabilization of $Cu^{1.5+}$-$Cu^{1.5+}$ versus Cu^{+}-Cu^{+}.[52,54]

Investigations using the *Pa*-Azu-Cu_A model indicate that E^0 may also be tuned trough second sphere mutation, i.e. by exchanging residues in the vicinity of the site that do not directly interact with the metal ions. Subsequent work based on loop engineering of *Tt*-Cu_A confirmed this observation and provided deeper insight into the determinants of E^0 regulation by outer sphere and coordinating amino acids. In these studies, the outer sphere was modified by replacing either one or the three loops that define the nearby environment of the metal site, but preserving in all cases the set of ligand residues (*Tt*-3L-*Hs*, *Tt*-3L-*At*, *Tt*-1L-E and *Tt*-1L-L chimeras in Table 1).[50,54] These conservative loop permutations impact E^0 in about ±35 mV (Table 1) that, as expected, is an effect significantly smaller than the one achieved with first sphere modifications. The magnitude of this modulation correlates with the hydrophobicity of the metal environment, which is estimated as the sum of hydrophobicity indexes for all residues belonging to the three surrounding loops. Also, in this case the enthalpy and entropy contributions to E^0 partially compensate each other, thereby attenuating the variation of E^0.

Interestingly, the introduction of the Met160His mutation into the *Tt*-3L-*Hs* chimera to produce the *Tt*-3L-M160H variant results in a downshift of E^0 with respect to WT *Tt*-Cu_A, which approximately corresponds to the sum of the downshifts induced by the individual first and second sphere modifications.[53]

As discussed in the preceding section, inner and outer sphere mutations of the *Tt*-Cu_A site result in modulation of $\Delta E_{\sigma_u^*/\pi_u}$, which is expected to have an impact on E^0 other than just coulombic stabilization/destabilization. Indeed, it was found that the reduction entropies of the different *Tt*-Cu_A variants, including first and second sphere modifications,

increase with $\Delta E_{\sigma_u^*/\pi_u}$. To rationalize this dependency, it should be considered that the oxidized Cu_A can be described in terms of two energy wells, the σ_u* and π_u states, both spin doublets. Thereby, the statistical weight of $Cu^{1.5+}$-$Cu^{1.5+}$ is determined by the $\Delta E_{\sigma_u^*/\pi_u}/k_BT$ ratio, with limiting values of 2 and 4 for very large and very small $\Delta E_{\sigma_u^*/\pi_u}$, respectively. The reduced form, on the other hand, is a spin singlet and is represented by a single well potential energy surface of orbital symmetry σ_u*. These simple considerations lead to the following expression for reduction entropy as a function of $\Delta E_{\sigma_u^*/\pi_u}$:

$$\Delta S = -k_B ln\left(2 + 2e^{-}\,\Delta E_{\sigma_u^*/\pi_u}/k_B T\right) + k_B ln(Q^*_{Red}/Q^*_{Ox}) \qquad \text{(Eq. 6)}$$

The first term in equation 6 accounts for changes in the electronic part of the partition function, while the second term corresponds to the non-electronic components. The modulation of the reduction entropy trough the thermal accessibility of the alternative electronic ground state π_u has been found to have an impact of up to 100 mV on the E^0 values of Cu_A variants.[52]

2.3. Electron transfer kinetic parameters of Cu_A

According to the theory (see Introduction), the ET rate constant is determined by electronic coupling and and reorganization energy, in addition to the thermodynamic driving force or redox potential. The coupling, in turn, is determined by the structural and dynamical features of the medium connecting donor and acceptor redox centers. The electronic pathways implicated in the inter- and intra-protein ET reactions of the redox hub Cu_A from CcO have been extensively investigated; yet a consensus description remains elusive.

In the case of bovine CcO, calculations of effective couplings combined with all-atom molecular dynamics of the membrane-embedded enzyme indicated that the most efficient pathway for intramolecular Cu_A→ heme *a* ET starts at the equatorial ligand His204, continues across one H-bond towards either Arg438 or Arg 439, and finally trough another H-bond to reach the heme *a* propionate (Figure 8).[62] An equivalent result was obtained for Cu_A→ heme *b* ET in the ba_3-CcO from *Thermus thermophilus*.[48]

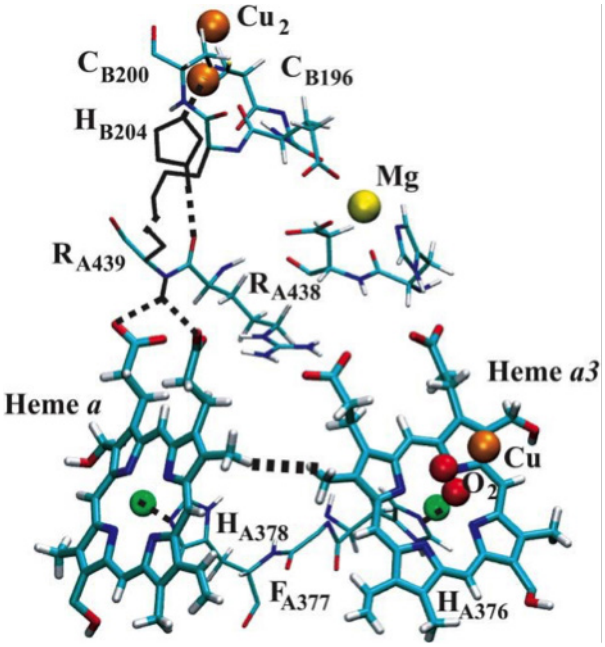

Figure 8. Intramolecular electron transfer pathways of CcO. Adopted from reference[62] with permission. Copyright 2003, Biophysical Society.

For the intermolecular Cyt-c→Cu_A ET reaction, calculations based on model and high resolution structures of the Cyt-c/CcO complex show that the most efficient pathway starts at either Trp104 or Tyr105 as electron entry gate, followed by a trough space jump to the weak axial ligand Met of the Cu_A center.[63] An equivalent route was predicted for the Cyt-c_{552}/*Tt*-Cu_A complex structure based on structures obtained by NMR and docking calculations.[64] Interestingly, quantum mechanical calculations show that the covalency of the Cu-S(Met), although low, is 10 times stronger in the π_u alternative GS relative to σ_u^*, which implies a ca. 100 times faster intermolecular ET reaction in the π_u state.[48] For the subsequent intramolecular ET step, the His pathway is favoured in the σ_u^* GS, as the covalency of the Cu- His bond is doubled compared to the π_u state. Taken together, these results suggest that the alternative π_u and σ_u^* ground states of Cu_A might be involved in effectively coupling upstream and downstream ET and in redirecting electrons by ca. 90°, as required by the geometry of the Cyt-c/CcO complex.[48]

ET reorganization energy has been experimentally determined for a few Cu_A proteins, including *Pa*-Azu-Cu_A, bovine CcO and *Tt*-Cu_A, yielding in all cases values around 0.3-0.4 eV.[1] Interestingly, these values are about a half of those determined for the related mononuclear T1 copper sites. This striking difference has been ascribed to the high electronic delocalization in Cu_A, which distributes redox-linked structural changes among twice the number of chemical bonds compared to mononuclear centers, thus reducing both the inner and outer sphere reorganization energies.

Quantum mechanical calculations performed assuming σ_u^* as the redox active molecular orbital afford λ values around 0.2-0.3 eV. Notably, this value doubles if the reaction proceeds from the alternative π_u GS, probably due to partial localization of the Cu_2S_2 covalence.[47,48]

Electrochemical experiments performed for a set of eight different *Tt*-Cu_A variants, including first and second sphere modifications (Figure 9), show clustering of the results in two groups, with average λ values of 0.53 ± 0.05 eV and 0.27 ± 0.05 eV, respectively.[54] The parameter that appears to determine membership of a particular protein variant to one or the other cluster is the energy gap $\Delta E_{\sigma_u^*/\pi_u}$, with small values around 12-256 cm^{-1} for the first group and significantly larger values around 440-900 cm^{-1} for the second one (Figure 9). Note that the first group includes variants that at room temperature present high populations of the alternative π_u GS, from ca. 25% up to full degeneracy (50 %). Moreover, the average λ obtained for this group closely resembles the QM prediction for the π_u GS. In the second group, in contrast, the average λ is very similar to the QM prediction for the σ_u^* GS, and protein variants included in this cluster have σ_u^* populations above 90 %. This clustering strongly suggest that the electrochemical experiments selectively probe one or the other redox active molecular orbital depending on the size of $\Delta E_{\sigma_u^*/\pi_u}$. Confirming this hypothesis, the M160H mutant falls into one or the other cluster depending on pH, which in turn has been found by UV-vis, EPR, RR and NMR to modulate $\Delta E_{\sigma_u^*/\pi_u}$ while preserving valence delocalization. Thus, experiments and calculations indicate that, for Cu_A variants with $\Delta E_{\sigma_u^*/\pi_u} > \Delta G_{ET}^{\#}$, the ET reaction proceeds from the lower-lying σ_u^* RAMO, while for centers with $\Delta E_{\sigma_u^*/\pi_u} < \Delta G_{ET}^{\#}$, the alternative π_u RAMO is preferentially involved. An important underlying implication of these results is that reaction coordinates for the ET reaction and for the $\sigma_u^* \rightarrow \pi_u$ conversion are strongly coupled. In line with this interpretation, the Cu-Cu distance is the main coordinate for the adiabatic $\sigma_u^* \rightarrow \pi_u$ transition, as demonstrated by QM calculations, and changes slightly with the redox state as determined by EXAFS.[54]

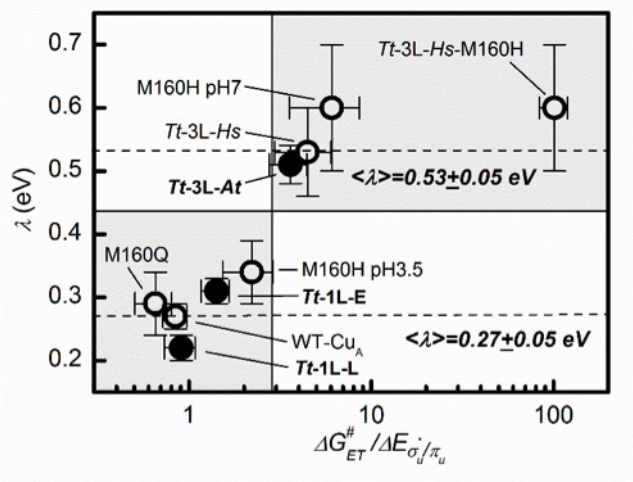

Figure 9. Electron transfer reorganization energy as a function of the ratio of ET activation energy divided by the energy gap between alternative ground states. Adopted with permission from reference [54]. Copyright 2019, American Chemical Society.

3. Regulation of Cyt-c→Cu_A intermolecular electron transfer

In the previous sections, I described some recent findings on the redox properties of Cyt-c and Cu_A metalloproteins. Here, I put these pieces of information together to hypothesize about a possible regulation mechanism of the Cyt-c→CcO ET reaction during electron-proton energy transduction in mitochondria (Figure 10).

When not associated, Cyt-c is in a native conformation of high λ value, which minimizes unwanted side redox reactions. Electrostatic binding to CcO leads to an initial complex that is not necessarily optimized in terms of heme *c*→Cu_A electron pathway and, therefore, reorientation of Cyt-c in the complex is required to enhance the electronic coupling. The electrostatic contacts in the complex induce subtle conformational distortions of Cyt-c (including disruption of the Met80/Tyr67 H-bond) that drive Cyt-c into a low λ native conformation that enables fast ET.

On the other hand, the idle form of the primary electron acceptor of CcO is largely dominated by the σ_u^* GS. Upon complex formation, subtle distortions of the Cu_A site induced by interaction with Cyt-c lower $\Delta E_{\sigma_u^*/\pi_u}$, favouring the π_u GS. This alternative GS accelerates heme *c*→Cu_A ET by two orders of magnitude compared to σ_u^* due to a more efficient mediation of the electronic coupling. The subsequent step is intramolecular ET from the reduced Cu_A site to heme *a* (or heme *b*, depending on the organism) in CcO. Electrons are redirected at ca. 90° abandoning the Cu_A site trough the His157 equatorial ligand. This pathway is favored by the σ_u^* GS due to a combination of enhanced *V* and lower λ. Thus, the alternation of electronic GS in Cu_A enable the switching of electron pathways that is required to ensure directionality despite the very low thermodynamic driving forces of the individual ET steps.

A temporary misbalance of proton translocation activity of respiratory complexes and consumption of the resulting electrochemical gradient by ATP-synthase may result in a deleterious hyperpolarization of the membrane. This, however, results in a rise of the local electric fields that may slow down the reorientation dynamics of Cyt-c in the complexes, thus undermining its ability to establish efficient electron pathways. Moreover, higher electric fields increase $\Delta E_{\sigma_u^*/\pi_u}$ in Cu_A, impairing the population of the most favorable electron entry gate, i.e. the π_u GS. Hence, the rise of the local electric field is expected to temporarily block or significantly slow down the proton-coupled ET reactions of the Cyt-c/CcO complex, until the electrochemical gradient is suffciently dissipated by ATP-synthase.

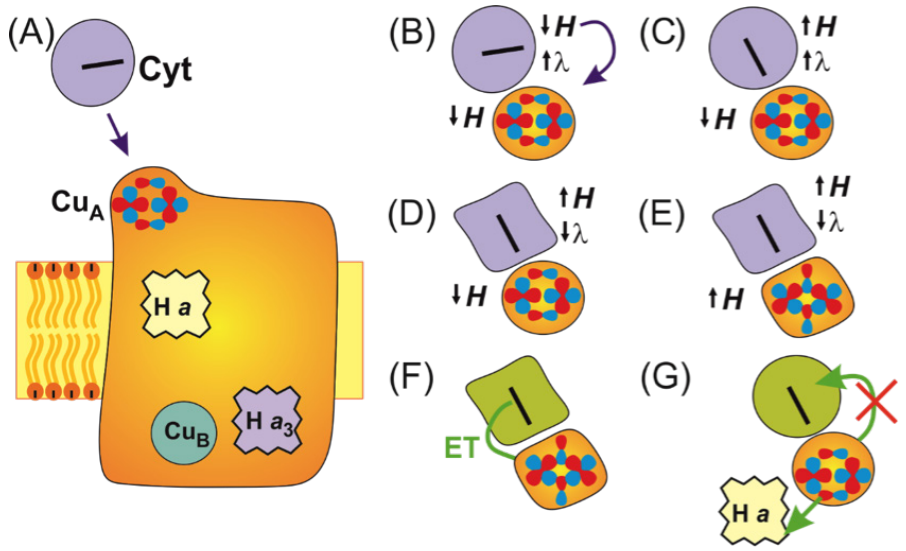

Figure 10. Schematic representation of the regulatory model for the Cyt-c/CcO ET reaction. Adopted from reference [32] with permission. Copyright 2014, Elsevier B.V. Cyt-c shuttles an electron towards the CcO, and docks near the Cu_A site (A). The complex is not optimized for ET so Cyt-c must reorient (B) in order to achieve a higher electronic coupling (C). In the process, more Cyt-c/CcO contacts are established, triggering a conformational transition of Cyt-c towards a lower λ form (D). The Cu_A site is perturbed in such a way that the π_u GS may be favored, thus further optimizing the electronic coupling (E). The ET reaction is then kinetically favored in spite of the low driving force and proceeds (F). Directionality is preserved and back ET is hampered because after the ET reaction the features that optimize the reaction are lost, and so the intramolecular ET towards heme *a* proceeds (G). Steps (B), (D) and (E) may be negatively affected by the strength of the interfacial electric field that increases because of the proton pumping resulting from the ET reactions. Thus, a regulatory negative feedback may be established due to the interplay between electron and proton transfer reactions. When the electric field lowers due to the activity of the ATP synthase, ET activity may be resumed.

Conclusions

Structural features such as first and second coordination spheres, local electrostatics and water accessibility are crucial determinants for the electronic properties of iron and copper metal sites in proteins, including thermodynamic and kinetic electron transfer parameters. The highly dynamical nature of proteins, in turn, enables the exploration of different structural and electronic configurations driven by thermal fluctuations. Moreover, specific electrostatic interactions, local electric fields and post-translational modifications reshape the free energy surfaces in a manner that may be central for the dynamic regulation of the canonical and alternative functions of metalloproteins. Understanding these complex mechanisms for the modulation of electron-proton energy transduction is essential from a basic biological and physicochemical perspective, but it is also a need for the successful development of metalloprotein-based technological devices such as biosensors, biofuel cells, enzymatic reactors and others.

Acknowledgment

Financial support by ANPCyT, UBACYT and CONICET is gratefully acknowledged.

References

[1] Liu, J.; Chakraborty, S.; Hosseinzadeh, P.; Yu, Y.; Tian, S.; Petrik, I.; Bhagi, A.; Lu, Y. Metalloproteins Containing Cytochrome, Iron-Sulfur, or Copper Redox Centers. *Chem. Rev.* **2014**, *114* (8), 4366–4369. https://doi.org/10.1021/cr400479b.

[2] Marcus, R. A.; Sutin, N. Electron Transfers in Chemistry and Biology. *BBA Rev. Bioenerg.* **1985**, *811* (3), 265–322. https://doi.org/10.1016/0304-4173(85)90014-X.

[3] Zitare, U. A.; Szuster, J.; Scocozza, M. F.; Espinoza-Cara, A.; Leguto, A. J.; Morgada, M. N.; Vila, A. J.; Murgida, D. H. The Role of Molecular Crowding in Long-Range Metalloprotein Electron Transfer: Dissection into Site- and Scaffold-Specific Contributions. *Electrochimica Acta* **2019**, *294*, 117–125. https://doi.org/10.1016/j.electacta.2018.10.069.

[4] Zitare, U. A.; Szuster, J.; Santalla, M. C.; Llases, M. E.; Morgada, M. N.; Vila, A. J.; Murgida, D. H. Fine Tuning of Functional Features of the CuA Site by Loop-Directed Mutagenesis. *Inorg. Chem.* **2019**. https://doi.org/10.1021/acs.inorgchem.8b03244.

[5] Beratan, D. N.; Onuchic, J. N.; Winkler; Gray, H. B. Electron-Tunneling Pathways in Proteins. *Science* **1992**, *258* (5089), 1740–1741. https://doi.org/10.1126/science.1334572.

[6] Alvarez-Paggi, D.; Hannibal, L.; Castro, M. A.; Oviedo-Rouco, S.; Demicheli, V.; Tórtora, V.; Tomasina, F.; Radi, R.; Murgida, D. H. Multifunctional Cytochrome c: Learning New Tricks from an Old Dog. *Chem. Rev.* **2017**, *117* (21), 13382–13460. https://doi.org/10.1021/acs.chemrev.7b00257.

[7] Bushnell, G. W.; Louie, G. V.; Brayer, G. D. High-Resolution Three-Dimensional Structure of Horse Heart Cytochrome c. *J. Mol. Biol.* **1990**, *214* (2), 585–595. https://doi.org/10.1016/0022-2836(90)90200-6.

[8] Hannibal, L.; Tomasina, F.; Capdevila, D. A.; Demicheli, V.; Tórtora, V.; Alvarez-Paggi, D.; Jemmerson, R.; Murgida, D. H.; Radi, R. Alternative Conformations of Cytochrome c: Structure, Function, and Detection. *Biochemistry* **2016**, *55* (3), 407–428. https://doi.org/10.1021/acs.biochem.5b01385.

[9] Capdevila, D. A.; Oviedo, R.; Tomasina, F.; Tortora, V.; Demicheli, V.; Radi, R.; Murgida, D. H. Active Site Structure and Peroxidase Activity of Oxidatively Modified Cytochrome c Species in Complexes with Cardiolipin. *Biochemistry* **2015**, *54* (51), 7491–7504. https://doi.org/10.1021/acs.biochem.5b00922.

[10] Capdevila, D. A.; Álvarez-Paggi, D.; Castro, M. A.; Tórtora, V.; Demicheli, V.; Estrín, D. A.; Radi, R.; Murgida, D. H. Coupling of Tyrosine Deprotonation and Axial Ligand Exchange in Nitrocytochrome c. *Chem. Commun.* **2014**, *50* (20), 2592–2594. https://doi.org/10.1039/C3CC47207H.

[11] Capdevila, D. A.; Marmisollé, W. A.; Tomasina, F.; Demicheli, V.; Portela, M.; Radi, R.; Murgida, D. H. Specific Methionine Oxidation of Cytochrome c in Complexes with Zwitterionic Lipids by Hydrogen Peroxide: Potential Implications for Apoptosis. *Chem. Sci.* **2015**, *6* (1), 705–713. https://doi.org/10.1039/c4sc02181a.

[12] Murgida, D. H.; Hildebrandt, P. Electron-Transfer Processes of Cytochrome c at Interfaces. New Insights by Surface-Enhanced Resonance Raman Spectroscopy. *Acc. Chem. Res.* **2004**, *37* (11), 854–861. https://doi.org/10.1021/ar0400443.

[13] Murgida, D. H.; Hildebrandt, P. Disentangling Interfacial Redox Processes of Proteins by SERR Spectroscopy. *Chem. Soc. Rev.* **2008**, *37* (5), 937–945. https://doi.org/10.1039/b705976k.

[14] Oviedo-Rouco, S.; Castro, M. A.; Alvarez-Paggi, D.; Spedalieri, C.; Tortora, V.; Tomasina, F.; Radi, R.; Murgida, D. H. The Alkaline Transition of Cytochrome c Revisited: Effects of Electrostatic Interactions and Tyrosine Nitration on the Reaction Dynamics. *Arch. Biochem. Biophys.* **2019**, *665*, 96–106. https://doi.org/10.1016/j.abb.2019.02.016.

[15] Yue, H.; Khoshtariya, D.; Waldeck, D. H.; Grochol, J.; Hildebrandt, P.; Murgida, D. H. On the Electron Transfer Mechanism Between Cytochrome c and Metal Electrodes. Evidence for Dynamic Control at Short Distances. *J. Phys. Chem. B* **2006**, *110* (40), 19906–19913. https://doi.org/10.1021/jp0620670.

[16] Murgida, D. H.; Hildebrandt, P. Electrostatic-Field Dependent Activation Energies Modulate Electron Transfer of Cytochrome c. *J. Phys. Chem. B* **2002**, *106* (49), 12814–12819. https://doi.org/10.1021/jp020762b.

[17] Alvarez-Paggi, D.; Castro, M. A.; Tórtora, V.; Castro, L.; Radi, R.; Murgida, D. H. Electrostatically Driven Second-Sphere Ligand Switch between High and Low Reorganization Energy Forms of Native Cytochrome c. *J. Am. Chem. Soc.* **2013**, *135* (11), 4389–4397. https://doi.org/10.1021/ja311786b.

[18] Paggi, D. A.; Martín, D. F.; Kranich, A.; Hildebrandt, P.; Martí, M. A.; Murgida, D. H. Computer Simulation and SERR Detection of Cytochrome c Dynamics at SAM-Coated Electrodes. *Electrochimica Acta* **2009**, *54* (22), 4963–4970. https://doi.org/10.1016/j.electacta.2009.02.050.

[19] Alvarez-Paggi, D.; Martín, D. F.; Debiase, P. M.; Hildebrandt, P.; Martí, M. A.; Murgida, D. H. Molecular Basis of Coupled Protein and Electron Transfer Dynamics of Cytochrome c in Biomimetic Complexes. *J. Am. Chem. Soc.* **2010**, *132* (16), 5769–5778. https://doi.org/10.1021/ja910707r.

[20] Murgida, D. H.; Hildebrandt, P. Heterogeneous Electron Transfer of Cytochrome c on Coated Silver Electrodes. Electric Field Effects on Structure and Redox Potential. *J. Phys. Chem. B* **2001**, *105* (8), 1578–1586.

[21] Khoa, L.; Wisitruangsakul, N.; Sezer, M.; Feng, J.-J.; Kranich, A.; Weidinger, I. M.; Zebger, I.; Murgida, D. H.; Hildebrandt, P. Electric-Field Effects on the Interfacial Electron Transfer and Protein Dynamics of Cytochrome c. *J. Electroanal. Chem.* **2011**, *660* (2), 367–376. https://doi.org/10.1016/j.jelechem.2010.12.020.

[22] Staffa, J. K.; Lorenz, L.; Stolarski, M.; Murgida, D. H.; Zebger, I.; Utesch, T.; Kozuch, J.; Hildebrandt, P. Determination of the Local Electric Field at Au/SAM Interfaces Using the Vibrational Stark Effect. *J. Phys. Chem. C* **2017**, *121* (40), 22274–22285. https://doi.org/10.1021/acs.jpcc.7b08434.

[23] Todorovic, S.; Murgida, D. H. Surface-Enhanced Raman Scattering of Biological Materials. In *Encyclopedia of Analytical Chemistry*; American Cancer Society, 2016; pp 1–29. https://doi.org/10.1002/9780470027318.a9574.

[24] Gu, J.; Yang, S.; Rajic, A. J.; Kurnikov, I. V.; Prytkova, T. R.; Pletneva, E. V. Control of Cytochrome c Redox Reactivity through Off-Pathway Modifications in the Protein Hydrogen-Bonding Network. *Chem. Commun.* **2014**, *50* (40), 5355–5357. https://doi.org/10.1039/C3CC47943A.

[25] Liptak, M. D.; Wen, X.; Bren, K. L. NMR and DFT Investigation of Heme Ruffling: Functional Implications for Cytochrome c. *J. Am. Chem. Soc.* **2010**, *132* (28), 9753–9763. https://doi.org/10.1021/ja102098p.

[26] Kranich, A.; Ly, H. K.; Hildebrandt, P.; Murgida, D. H. Direct Observation of the Gating Step in Protein Electron Transfer: Electric-Field-Controlled Protein Dynamics. *J. Am. Chem. Soc.* **2008**, *130* (30), 9844–9848. https://doi.org/10.1021/ja8016895.

[27] Wisitruangsakul, N.; Zebger, I.; Ly, K. H.; Murgida, D. H.; Ekgasit, S.; Hildebrandt, P. Redox-Linked Protein Dynamics of Cytochrome c Probed by Time-Resolved Surface Enhanced Infrared Absorption Spectroscopy. *Phys. Chem. Chem. Phys.* **2008**, *10* (34), 5276–5286. https://doi.org/10.1039/b806528d.

[28] Ly, H. K.; Marti, M. A.; Martin, D. F.; Alvarez-Paggi, D.; Meister, W.; Kranich, A.; Weidinger, I. M.; Hildebrandt, P.; Murgida, D. H. Thermal Fluctuations Determine the Electron-Transfer Rates of Cytochrome c in Electrostatic and Covalent Complexes. *ChemPhysChem* **2010**, *11* (6), 1225–1235. https://doi.org/10.1002/cphc.200900966.

[29] Capdevila, D. A.; Marmisollé, W. A.; Williams, F. J.; Murgida, D. H. Phosphate Mediated Adsorption and Electron Transfer of Cytochrome c. A Time-Resolved SERR Spectroelectrochemical Study. *Phys. Chem. Chem. Phys.* **2013**, *15* (15), 5386–5394. https://doi.org/10.1039/c2cp42044a.

[30] Alvarez-Paggi, D.; Meister, W.; Kuhlmann, U.; Weidinger, I.; Tenger, K.; Zimányi, L.; Rákhely, G.; Hildebrandt, P.; Murgida, D. H. Disentangling Electron Tunneling and Protein Dynamics of Cytochrome c through a Rationally Designed Surface Mutation. *J. Phys. Chem. B* **2013**, *117* (20), 6061–6068. https://doi.org/10.1021/jp400832m.

[31] Murgida, D. H.; Hildebrandt, P. Redox and Redox-Coupled Processes of Heme Proteins and Enzymes at Electrochemical Interfaces. *Phys. Chem. Chem. Phys.* **2005**, *7* (22), 3773–3784. https://doi.org/10.1039/b507989f.

[32] Alvarez-Paggi, D.; Zitare, U.; Murgida, D. H. The Role of Protein Dynamics and Thermal Fluctuations in Regulating Cytochrome c/Cytochrome c Oxidase Electron Transfer. *Biochim. Biophys. Acta - Bioenerg.* **2014**, *1837* (7), 1196–1207. https://doi.org/10.1016/j.bbabio.2014.01.019.

[33] Murgida, D. H.; Hildebrandt, P.; Wei, J.; He, Y.-F.; Liu, H.; Waldeck, D. H. Surface-Enhanced Resonance Raman Spectroscopic and Electrochemical Study of Cytochrome c Bound on Electrodes through Coordination with Pyridinyl-Terminated Self-Assembled Monolayers. *J. Phys. Chem. B* **2004**, *108* (7), 2261–2269.

[34] Oellerich, S.; Wackerbarth, H.; Hildebrandt, P. Spectroscopic Characterization of Nonnative Conformational States of Cytochrome c. *J. Phys. Chem. B* **2002**, *106* (25), 6566–6580. https://doi.org/10.1021/jp013841g.

[35] Kroll, T.; Hadt, R. G.; Wilson, S. A.; Lundberg, M.; Yan, J. J.; Weng, T.-C.; Sokaras, D.; Alonso-Mori, R.; Casa, D.; Upton, M. H.; et al. Resonant Inelastic X-Ray Scattering on Ferrous and Ferric Bis-Imidazole Porphyrin and Cytochrome c: Nature and Role of the Axial Methionine–Fe Bond. *J. Am. Chem. Soc.* **2014**, *136* (52), 18087–18099. https://doi.org/10.1021/ja5100367.

[36] Mara, M. W.; Hadt, R. G.; Reinhard, M. E.; Kroll, T.; Lim, H.; Hartsock, R. W.; Alonso-Mori, R.; Chollet, M.; Glownia, J. M.; Nelson, S.; et al. Metalloprotein Entatic Control of Ligand-Metal Bonds Quantified by Ultrafast x-Ray Spectroscopy. *Science* **2017**, *356* (6344), 1276–1280. https://doi.org/10.1126/science.aam6203.

[37] De, B.; Doctorovich, F.; Murgida, D. H.; Estrin, D. A. Electric Field Effects on the Reactivity of Heme Model Systems. *Chem. Phys. Lett.* **2007**, *434* (1–3), 121–126. https://doi.org/10.1016/j.cplett.2006.11.104.

[38] De, B.; Paggi, D. A.; Doctorovich, F.; Hildebrandt, P.; Estrin, D. A.; Murgida, D. H.; Marti, M. A. Molecular Basis for the Electric Field Modulation of Cytochrome c Structure and Function. *J. Am. Chem. Soc.* **2009**, *131* (44), 16248–16256. https://doi.org/10.1021/ja906726n.

[39] Assfalg, M.; Bertini, I.; Dolfi, A.; Turano, P.; Mauk, A. G.; Rosell, F. I.; Gray, H. B. Structural Model for an Alkaline Form of Ferricytochrome c. *J. Am. Chem. Soc.* **2003**, *125* (10), 2913–2922. https://doi.org/10.1021/ja027180s.

[40] Amacher, J. F.; Zhong, F.; Lisi, G. P.; Zhu, M. Q.; Alden, S. L.; Hoke, K. R.; Madden, D. R.; Pletneva, E. V. A Compact Structure of Cytochrome c Trapped in a Lysine-Ligated State: Loop Refolding and Functional Implications of a Conformational Switch. *J. Am. Chem. Soc.* **2015**, *137* (26), 8435–8449. https://doi.org/10.1021/jacs.5b01493.

[41] Abriata, L. A.; Cassina, A.; Tórtora, V.; Marín, M.; Souza, J. M.; Castro, L.; Vila, A. J.; Radi, R. Nitration of Solvent-Exposed Tyrosine 74 on Cytochrome c Triggers Heme Iron-Methionine 80 Bond Disruption. Nuclear Magnetic Resonance and Optical Spectroscopy Studies. *J. Biol. Chem.* **2009**, *284* (1), 17–26. https://doi.org/10.1074/jbc.M807203200.

[42] Wackerbarth, H.; Murgida, D. H.; Oellerich, S.; Döpner, S.; Rivas, L.; Hildebrandt, P. Dynamics and Mechanism of the Electron Transfer Process of Cytochrome c Probed by Resonance Raman and Surface Enhanced Resonance Raman Spectroscopy. *J. Mol. Struct.* **2001**, *563–564*, 51–59. https://doi.org/10.1016/S0022-2860(00)00808-5.

[43] Kagan, V. E.; Bayır, H. A.; Belikova, N. A.; Kapralov, O.; Tyurina, Y. Y.; Tyurin, V. A.; Jiang, J.; Stoyanovsky, D. A.; Wipf, P.; Kochanek, P. M.; et al. Cytochrome c/Cardiolipin Relations in Mitochondria: A Kiss of Death. *Free Radic. Biol. Med.* **2009**, *46* (11), 1439–1453. https://doi.org/10.1016/j.freeradbiomed.2009.03.004.

[44] Liu, B.; Chen, Y.; Doukov, T.; Soltis, S. M.; Stout, C. D.; Fee, J. A. Combined Microspectrophotometric and Crystallographic Examination of Chemically Reduced and X-Ray Radiation-Reduced Forms of Cytochrome Ba3 Oxidase from Thermus Thermophilus: Structure of the Reduced Form of the Enzyme. *Biochemistry* **2009**, *48* (5), 820–826. https://doi.org/10.1021/bi801759a.

[45] Williams, P. A.; Blackburn, N. J.; Sanders, D.; Bellamy, H.; Stura, E. A.; Fee, J. A.; McRee, D. E. The Cu_A Domain of *Thermus Thermophilus* Ba_3-Type Cytochrome *c* Oxidase at 1.6 Å Resolution. *Nat. Struct. Mol. Biol.* **1999**, *6* (6), 509–516. https://doi.org/10.1038/9274.

[46] Solomon, E. I.; Heppner, D. E.; Johnston, E. M.; Ginsbach, J. W.; Cirera, J.; Qayyum, M.; Kieber-Emmons, M. T.; Kjaergaard, C. H.; Hadt, R. G.; Tian, L. Copper Active Sites in Biology. *Chem. Rev.* **2014**, *114* (7), 3659–3853. https://doi.org/10.1021/cr400327t.

[47] Gorelsky, S. I.; Xie, X.; Chen, Y.; Fee, J. A.; Solomon, E. I. The Two-State Issue in the Mixed-Valence Binuclear CuA Center in Cytochrome c Oxidase and N2O Reductase. *J. Am. Chem. Soc.* **2006**, *128* (51), 16452–16453. https://doi.org/10.1021/ja067583i.

[48] Abriata, L. A.; Álvarez-Paggi, D.; Ledesma, G. N.; Blackburn, N. J.; Vila, A. J.; Murgida, D. H. Alternative Ground States Enable Pathway Switching in Biological Electron Transfer. *Proc. Natl. Acad. Sci. U. S. A.* **2012**, *109* (43), 17348–17353. https://doi.org/10.1073/pnas.1204251109.

[49] Ledesma, G. N.; Murgida, D. H.; Hoang, K. L.; Wackerbarth, H.; Ulstrup, J.; Costa-Filho, A. J.; Vila, A. J. The Met Axial Ligand Determines the Redox Potential in CuA Sites. *J. Am. Chem. Soc.* **2007**, *129* (39), 11884–11885. https://doi.org/10.1021/ja0731221.

[50] Morgada, M. N.; Abriata, L. A.; Zitare, U.; Alvarez-Paggi, D.; Murgida, D. H.; Vila, A. J. Control of the Electronic Ground State on an Electron-Transfer Copper Site by Second-Sphere Perturbations. *Angew. Chem. - Int. Ed.* **2014**, *53* (24), 6188–6192. https://doi.org/10.1002/anie.201402083.

[51] Zitare, U.; Alvarez-Paggi, D.; Morgada, M. N.; Abriata, L. A.; Vila, A. J.; Murgida, D. H. Reversible Switching of Redox-Active Molecular Orbitals and Electron Transfer Pathways in CuA Sites of Cytochrome c Oxidase. *Angew. Chem. - Int. Ed.* **2015**, *54* (33), 9555–9559. https://doi.org/10.1002/anie.201504188.

[52] Alvarez-Paggi, D.; Zitare, U. A.; Szuster, J.; Morgada, M. N.; Leguto, A. J.; Vila, A. J.; Murgida, D. H. Tuning of Enthalpic/Entropic Parameters of a Protein Redox Center through Manipulation of the Electronic Partition Function. *J. Am. Chem. Soc.* **2017**, *139* (29), 9803–9806. https://doi.org/10.1021/jacs.7b05199.

[53] Leguto, A. J.; Smith, M. A.; Morgada, M. N.; Zitare, U. A.; Murgida, D. H.; Lancaster, K. M.; Vila, A. J. Dramatic Electronic Perturbations of CuA Centers via Subtle Geometric Changes. *J. Am. Chem. Soc.* **2019**, *141* (3), 1373-1381. https://doi.org/10.1021/jacs.8b12335.

[54] Zitare, U. A.; Szuster, J.; Santalla, M. C.; Llases, M. E.; Morgada, M. N.; Vila, A. J.; Murgida, D. H. Fine Tuning of Functional Features of the CuA Site by Loop-Directed Mutagenesis. *Inorg. Chem.* **2019**, *58*, 2149–2157. https://doi.org/10.1021/acs.inorgchem.8b03244.

[55] Hwang, H. J.; Lu, Y. PH-Dependent Transition between Delocalized and Trapped Valence States of a CuA Center and Its Possible Role in Proton-Coupled Electron Transfer. *Proc. Natl. Acad. Sci.* **2004**, *101* (35), 12842–12847. https://doi.org/10.1073/pnas.0403473101.

[56] Xie, X.; Gorelsky, S. I.; Sarangi, R.; Garner, D. K.; Hwang, H. J.; Hodgson, K. O.; Hedman, B.; Lu, Y.; Solomon, E. I. Perturbations to the Geometric and Electronic Structure of the CuA Site: Factors That Influence Delocalization

and Their Contributions to Electron Transfer. *J. Am. Chem. Soc.* **2008**, *130* (15), 5194–5205. https://doi.org/10.1021/ja7102668.

[57] Alvarez-Paggi, D.; Abriata, L. A.; Murgida, D. H.; Vila, A. J. Native CuA Redox Sites Are Largely Resilient to PH Variations within a Physiological Range. *Chem. Commun.* **2013**, *49* (47), 5381–5383. https://doi.org/10.1039/c3cc40457a.

[58] Clark, K. M.; Tian, S.; Donk, W. A. van der; Lu, Y. Probing the Role of the Backbone Carbonyl Interaction with the CuA Center in Azurin by Replacing the Peptide Bond with an Ester Linkage. *Chem. Commun.* **2016**, *53* (1), 224–227. https://doi.org/10.1039/C6CC07274G.

[59] Hwang, H. J.; Berry, S. M.; Nilges, M. J.; Lu, Y. Axial Methionine Has Much Less Influence on Reduction Potentials in a CuA Center than in a Blue Copper Center. *J. Am. Chem. Soc.* **2005**, *127* (20), 7274–7275. https://doi.org/10.1021/ja0501114.

[60] Wang, K.; Geren, L.; Zhen, Y.; Ma, L.; Ferguson-Miller, S.; Durham, B.; Millett, F. Mutants of the CuA Site in Cytochrome c Oxidase of Rhodobacter Sphaeroides: II. Rapid Kinetic Analysis of Electron Transfer. *Biochemistry* **2002**, *41* (7), 2298–2304. https://doi.org/10.1021/bi0114630.

[61] Zickermann, V.; Verkhovsky, M.; Morgan, J.; Wikström, M.; Anemüller, S.; Bill, E.; Steffens, G. C. M.; Ludwig, B. Perturbation of the CuA Site in Cytochrome-c Oxidase of Paracoccus Denitrificans by Replacement of Met227 with Isoleucine. *Eur. J. Biochem.* **1995**, *234* (2), 686–693. https://doi.org/10.1111/j.1432-1033.1995.686_b.x.

[62] Tan, M.-L.; Balabin, I.; Onuchic, J. N. Dynamics of Electron Transfer Pathways in Cytochrome c Oxidase. *Biophys. J.* **2004**, *86* (3), 1813–1819. https://doi.org/10.1016/S0006-3495(04)74248-4.

[63] Shimada, S.; Shinzawa-Itoh, K.; Baba, J.; Aoe, S.; Shimada, A.; Yamashita, E.; Kang, J.; Tateno, M.; Yoshikawa, S.; Tsukihara, T. Complex Structure of Cytochrome c–Cytochrome c Oxidase Reveals a Novel Protein–Protein Interaction Mode. *EMBO J.* **2017**, *36* (3), 291–300. https://doi.org/10.15252/embj.201695021.

[64] Muresanu, L.; Pristovsek, P.; Löhr, F.; Maneg, O.; Mukrasch, M. D.; Rüterjans, H.; Ludwig, B.; Lücke, C. The Electron Transfer Complex between Cytochrome C552 and the CuA Domain of the Thermus Thermophilus ba3 Oxidase A Combined NMR and computational approach. *J. Biol. Chem.* **2006**, *281* (20), 14503–14513. https://doi.org/10.1074/jbc.M601108200.

Bio

Daniel H. Murgida

Daniel H. Murgida received his PhD in Chemistry in 1997 from the School of Sciences of the University of Buenos Aires. He has been Visiting Scientist at the University of Parma, Humboldt Fellow at the Max Planck Institute for Radiation Chemistry, Staff Scientist at the New University of Lisbon, and Assistant Professor at the Technical University of Berlin. Since 2007 he is a Professor and CONICET Researcher at the University of Buenos Aires. His research focuses on structure-dynamics-function relationships that determine redox and alternative functions of metalloproteins, and combines theoretical and experimental approaches, mainly protein electrochemistry, spectroscopy and vibrational spectroelectrochemistry.